# First results of simulations with COSMO-1˙ITA and comparison of results with COSMO configurations at different resolutions

M. P. Manzi[1], P. Mercogliano[1,2] and M. Milelli[3]

*1 Impact on soil and Coast Division, EuroMediterranean Centre for Climate Change (CMCC),I-81043 Capua (CE), Italy*
*2 Meteo System & Instrumentation Laboratory, Italian Aerospace Research Center (CIRA), I-81043 Capua (CE), Italy*
*3 ARPA Piemonte, I-10135 Torino, Italy*

## 1 Introduction

In the framework of the project COSMO-NExT, a configuration of COSMO at 1.1 km of resolution (named COSMO-1) is under development at MeteoSwiss. COSMO-1 has also been used at CIRA, for the realization of some tests, in collaboration with MeteoSwiss and ARPA Piemonte. The first aim of this work concerned the testing of this particular configuration over the Italian domain for a 6 days period. This configuration has been named COSMO-1_ITA. A preliminary activity was constituted by optimization of parameters, mainly concerning the numerics, for the selected domain. Furthermore, to evaluate the performances of the COSMO-1_ITA configuration, different typology of observations have been used for the validation: satellite data and radio soundings, in order to evaluate the configuration performances respectively in the upper layers and through the different layers of atmosphere. Furthermore, a comparison of the results has been realized comparing the output of the 1km simulation with configuration of COSMO at different resolutions: 2.8km and 7km. The last analysis performed over COSMO-1_ITA simulation's results has been the analysis of the kinetic energy spectra to locate the effective resolution of the run.

## 2 Description of the test cases and features of the simulation

The test case interested a 6 days period, from $25^{th}$ to $30^{th}$ of November 2012. The synoptical situation during these six days was quite diversified: in the first day the Mediterranean area was interested by a high pressure ridge (Figure 1) that, in the following days, gradually collapsed pushed towards Eastern Europe by an Atlantic perturbation (Figure 2).

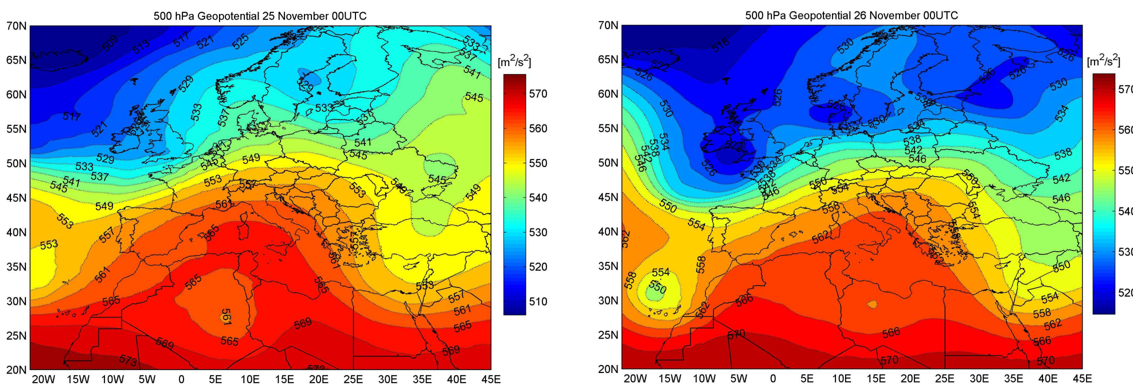


(a) (b)

Figure 1: Geopotential at 500hPa for $25^{th}$, $26^{th}$ at 00UTC. Data taken from the analysis at 00UTC of the ECMWF global model.

From the afternoon of $27^{th}$ to $30^{th}$ of November 2012, indeed, Italy was interested by an intense southern moist flow due to a low pressure system centred over the western Mediterranean Sea. This synoptic pattern caused an intense thunderstorm activity with widespread precipitations over the peninsula. The precipitation over the southern Italy, on which the simulation domain is centred, started the 27th of November.

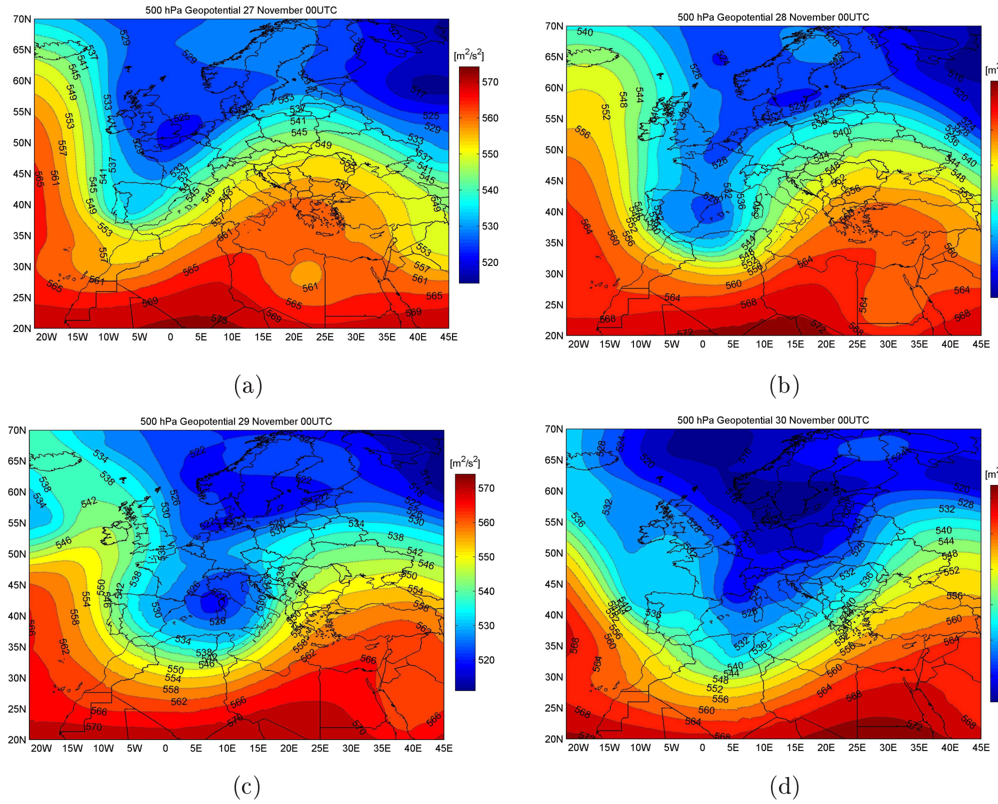


Figure 2: Geopotential at 500hPa for $27^{th}$, $28^{th}$, $29^{th}$, and $30^{th}$ at 00UTC. Data taken from the analysis at 00UTC of the ECMWF global model.

The choise of this period, then, due to the high variety of weather conditions, made it possible to evaluate the performance of the model under various meteorological conditions.

The nesting strategy used to perform the simulations is shown in Figure 3. The boundary and initial condition for the 7km simulations (COSMO-7_ITA) are taken from the forecast of the T1279 ECMWF model. The output obtained from COSMO-7_ITA is used to initialize the simulations performed with COSMO at 2.8km of resolution (COSMO-2.8_ITA) and with COSMO-1_ITA.

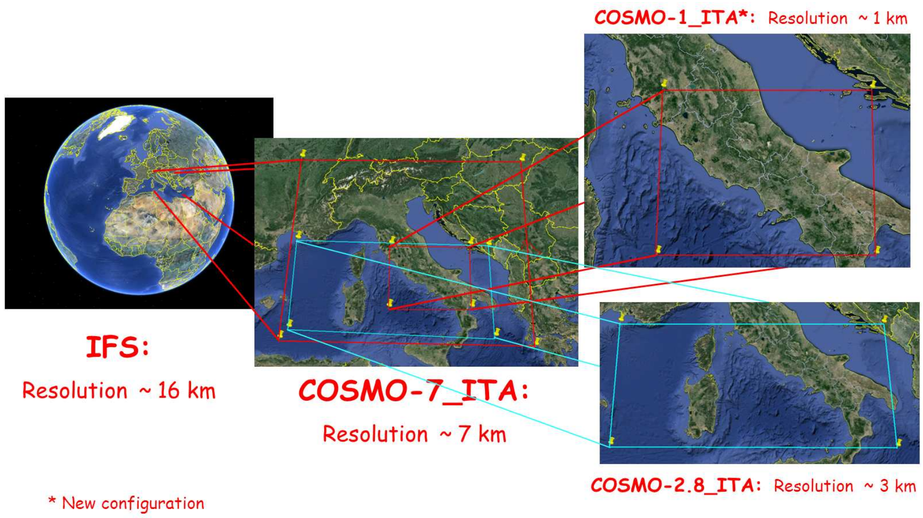


Figure 3: Nesting strategy used for COSMO-7_ITA, COSMO-2.8_ITA, COSMO-1_ITA configurations.

In Figure 3, in the upper right image, is shown the computational domain used for the optimized version of 1km simulations. A first optimization, indeed, interested the selection of the domain's dimension: the new simulations of COSMO-1_ITA were performed on a bigger domain. In Figure 4 is shown the difference between old (a) and new (b) domain.

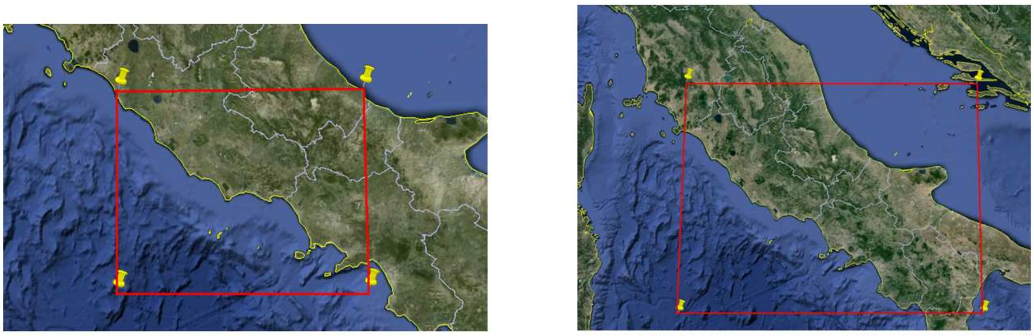

(a) (b)

Figure 4: Comparison between old (a) and new (b) domain.

Moreover, some parameters in model dynamics have been changed (Baldauf, 2010). Some of the most relevant settings for the two configurations are shown below in Table 1.

| **Parameter name** | **New configuration** | **Old configuration** |
|---|---|---|
| Grid characteristic | ie_tot=400, je_tot=300, ke_tot=60 | ie_tot=225, je_tot=120, ke_tot=60 |
| Time step (s) | dt = 5.0 | dt = 5.0 |
| Coefficient for divergence damping | xkd=0.1 | xkd=0.01 |
| Fast wave solver | itype_fast_waves=2 | itype_fast_waves=2 |
| Bottom boundary condition | itype_bbc_w=114 | itype_bbc_w=4 |
| Runge Kutta advection scheme | iadv_order=5 | iadv_order=5 |

Table 1: Namelist comparison between old and new (optimized) versions of COSMO-1_ITA.

To summarize, the most important settings choosen for each one of the three configuration are reported below in Table 2.

| **Parameter name** | **7km** | **2.8km** | **1.1km** |
|---|---|---|---|
| Grid characteristic | ie_tot=240, je_tot=160, ke_tot=40 | ie_tot=400, je_tot=175, ke_tot=60 | ie_tot=400, je_tot=300, ke_tot=60 |
| Time step (s) | dt = 40.0 | dt = 20.0 | dt = 5.0 |
| Interval between two consecutive boundary data | hincbound=3.0 | hincbound=1.0 | hincbound=1.0 |
| Subgrid-scale convection | lconv=.true., itype_conv=0, | lconv=.true., itype_conv=3, | lconv=.true., itype_conv=3, |
| Switch for nudging | lnudge =.TRUE., | lnudge =.FALSE., | lnudge =.FALSE., |

Table 2: Comparison between parameters settings for the three configurations.

The number of vertical levels has been increased from $40^{th}$ for the 7km run to $60^{th}$ for 2.8km/1.1km runs. In Figure 5 is reported the distribution of the vertical levels described above. Anyhow no further investigation has been carried out in this work about the number of the vertical levels to be used in COSMO-1_ITA, since previous studies show that the model behavior substantially does not change, changing the number of vertical levels (Milelli, 2012).

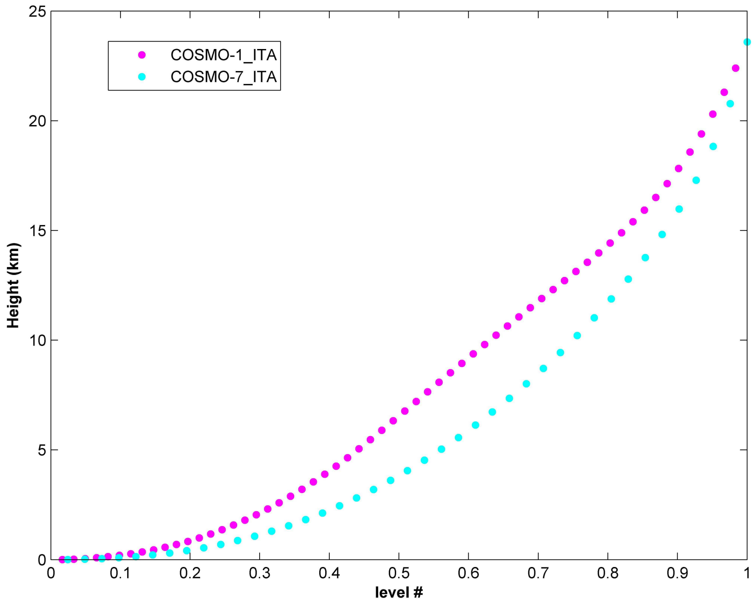


Figure 5: Distribution of the vertical levels for COSMO-7_ITA and COSMO-1_ITA configurations. Note that the same distribution of COSMO-1_ITA has been used even for COSMO-2.8_ITA.

The assimilation is performed through the use of the nudging technique only for the 7km simulations. As reported in Figure 6, at 12UTC a simulation of COSMO-7_ITA has been realized with a forecast range of 12 hours and with assimilation enabled. The output of this run has been included in the initial conditions of COSMO-7_ITA at 00UTC. In their turn the outputs of the 7km run at 00UTC have been used for the nesting of 1km and 2.8km runs, performed only at 00UTC.

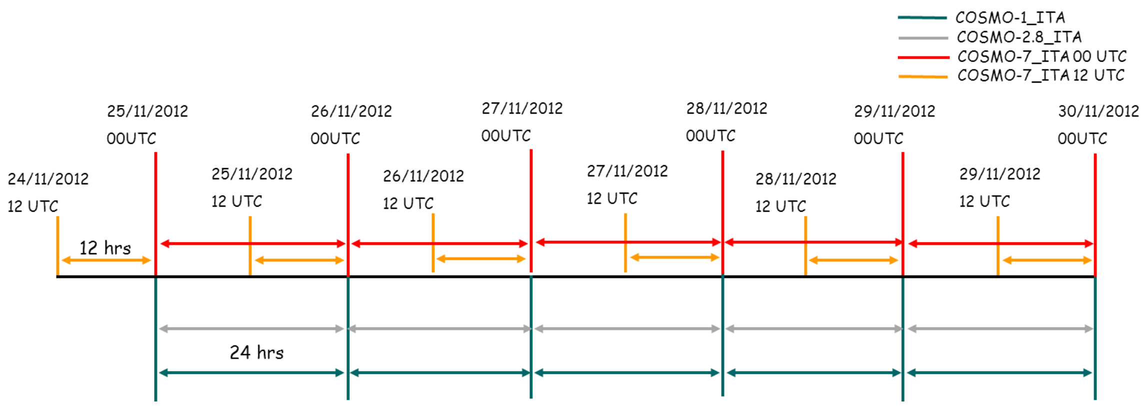


Figure 6: Scheme of performed simulations.

The increasing in spatial resolution means also a more accurate description of the analyzed domain characterized by a complex orography in which are present, at very low distance, Mediterranean Sea and Appennines (Figure 7).

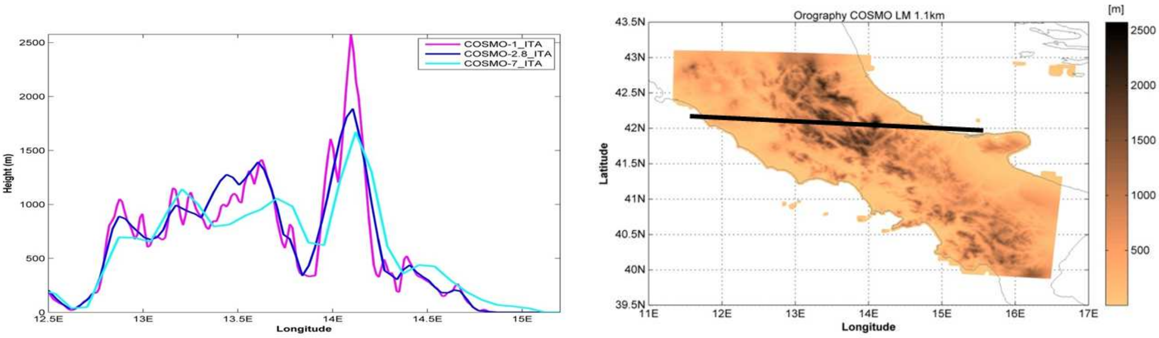


Figure 7: Comparison between the three orographies of the three simulations at the fixed latitude of $42^o$.

There is therefore the necessity of a proper treatment of orography and filtering in the passage from 7km to 2.8km and 1km. In the Table 3 are reported the main characteristics for orography filtering.

| **Parameter name** | **int2lm 7km - 1km and int2lm 7km - 2.8km** |
|---|---|
| Type of low pass filter<br>and number of sequential<br>applications of filter | lfilter_oro=.true.,<br>ilow_pass_oro=4,<br>numfilt_oro=1, |
| Parameter for filtering and<br>order of the orography filtering | eps_filter=0.1,<br>norder_filter=5, |
| Extra smoothing<br>of steep orography | ilow_pass_xso=6,<br>lxso_first=.FALSE.,<br>numfilt_xso=6,<br>rxso_mask=300.0, |

Table 3: Treatment of orography and filtering in int2lm.

## 3 Performances evaluation

The performances evaluation has been realized through the use of satellite images and sounding data. The observed satellite data have been provided by courtesy of University of Sannio, while sounding data were freely available on internet. The decision to use these two different types of data is derived from the specific characteristics that belong to each of them and that in some ways make them complementary.

Indeed, although satellite data have the great advantage of high resolution in space and time and give information of the weather in areas where no other observations are available, the use of satellite data offers only the possibility to make an analysis of the situation of the upper part of the atmosphere. For this reason a second kind of validation has been performed.

In order to better understand the behavior of the atmosphere also through the different layers, the second part of the validation work has been carried out through the comparison of observed soundings and simulated soundings obtained from the three simulations.

As regards the comparison via satellite images, two channels have been used: 10.8 $\mu$m (infrared channel) and 6.2 $\mu$m (water vapor channel), which are typically used for the detection of clouds. The results have been analyzed for two particular cases: one cloudless and the other one cloudy which show, respectively, the best and the worst results. In Figure 8 are shown the differences between observed and synthetic satellite images (Saunders, 2008 and 1999), for the three simulations (column-wise) and for the two considered channels (row-wise) for the 4th hour of forecast of $26^{th}$ November. In this case the error is quite low for all the simulations, for both channels.

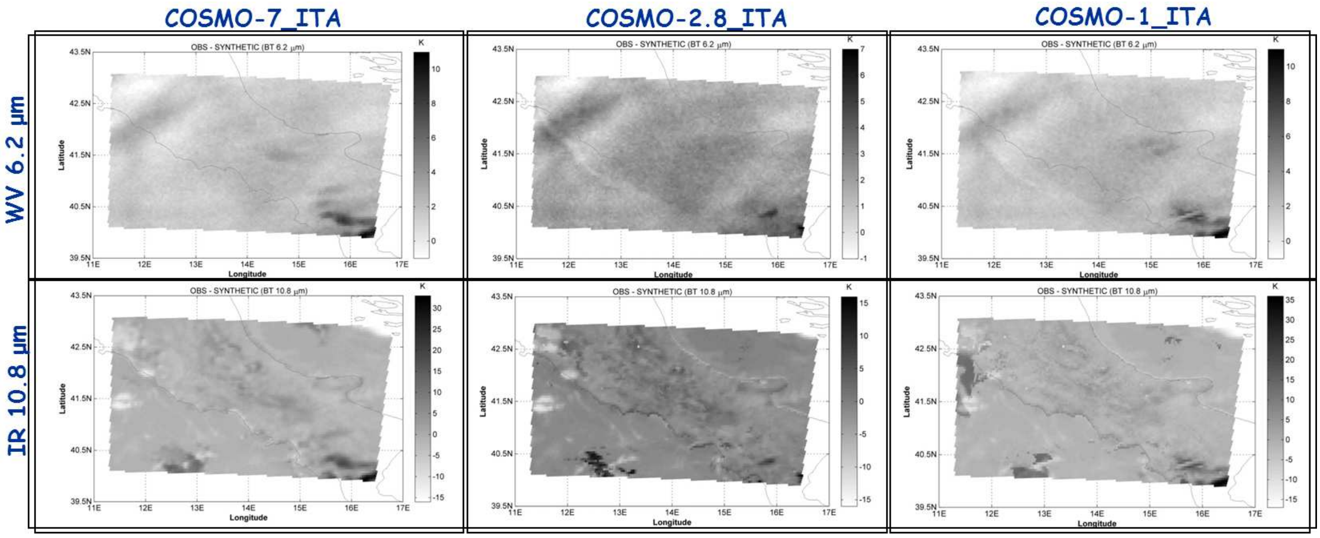


Figure 8: Comparison of observed and synthetic satellite images for the three simulations, in the two selected channels, for $26^{th}$ November 2012 at 04UTC.

In Figure 9 are shown the differences for the $13^{th}$ hour of forecast of $30^{th}$ November. In this case, especially for the 10.8 $\mu$m channel, the error is higher for all the simulations: white areas in the images (highlighted by red circles) denote values of model higher than observed, in other words the model is hotter than reality; dark areas (highlighted by blue circles), instead, denote model values lower than observed, in this case the model is colder.

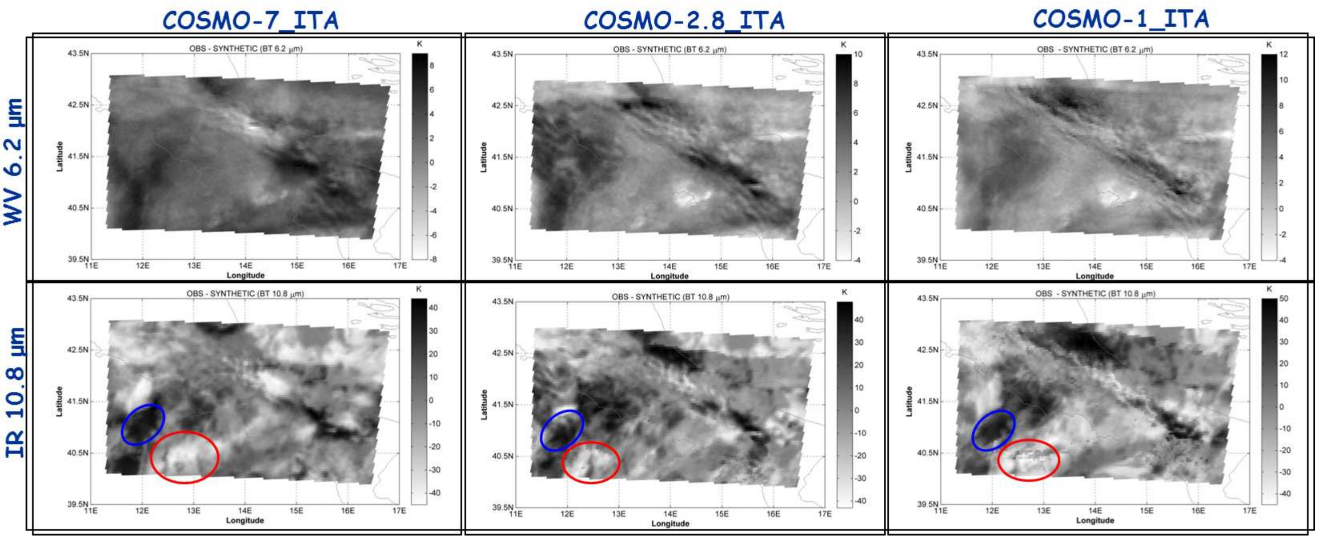


Figure 9: Comparison of observed and synthetic satellite images for the three simulations, in the two selected channels, for $30^{th}$ November 2012 at 13UTC.

To summarize the results obtained for all the days of simulation two statistical indices have been calculated, as described in Reichert et al., 2005. The first is the correlation coefficient, calculated as reported in (1):

$$r = \frac{\sum (x_i - \bar{x})(y_i - \bar{y})}{\sqrt{\sum_{i=1}^{n} (x_i - \bar{x})^2 \sum_{i=1}^{n} (y_i - \bar{y})^2}} \tag{1}$$

where x are pixel values of the synthetic image, y are the pixel values of the observed image and n is the number of pixels in image. The second index used is the Root Mean Square Error, calculated as in (2):

$$RMSE = \sqrt{\frac{\sum_{i=1}^{n} (x_i - \hat{x})^2}{n}} \tag{2}$$

where x are the pixel values of the observed image, $\hat{x}$ are the pixel values of the synthetic image and n is the number of pixels in image.

In Figure 10 is reported the comparison between the correlation coefficients of the three simulations for the 10.8 $mu$m channel (upper image) and the 6.2 $mu$m channel (lower image).

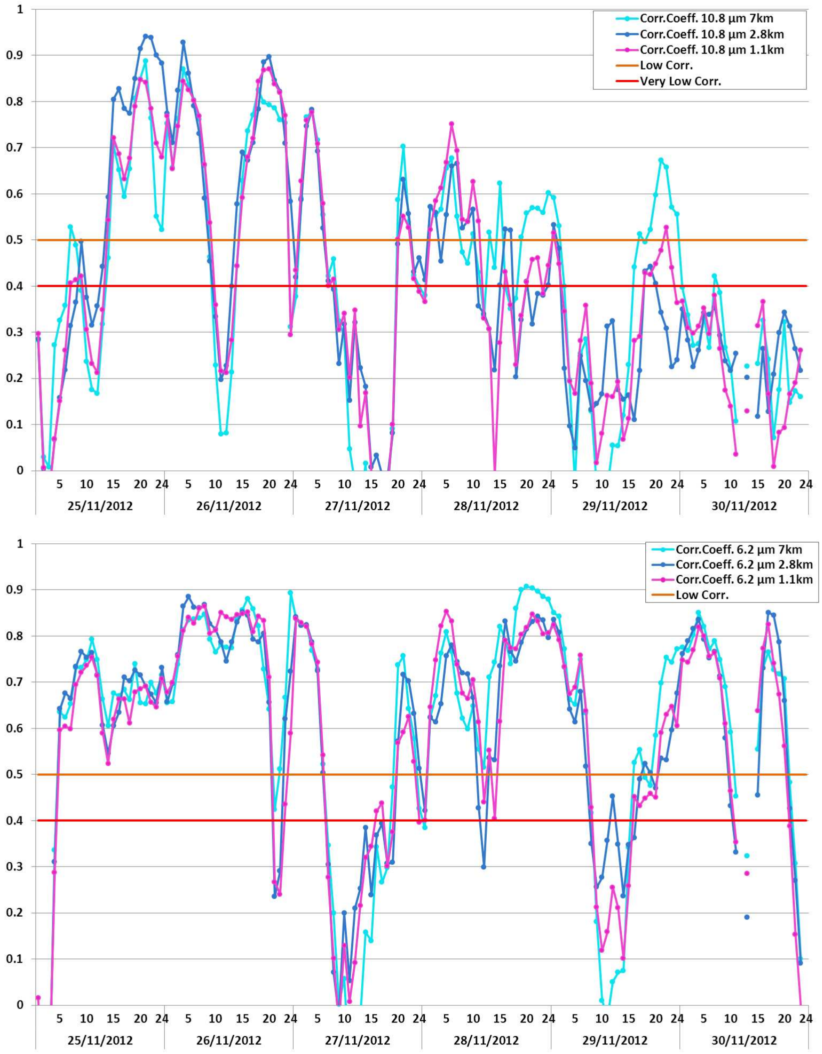


**Mean Corr.Coeff. 10.8 µm**

| | 25 | 26 | 27 | 28 | 29 | 30 |
|---|---|---|---|---|---|---|
| **7km** | 0,46 | 0,62 | 0,32 | 0,51 | 0,32 | 0,25 |
| **2.8km** | 0,52 | 0,67 | 0,36 | 0,44 | 0,25 | 0,26 |
| **1.1km** | 0,46 | 0,64 | 0,36 | 0,45 | 0,29 | 0,22 |

**Mean Corr.Coeff. 6.2 µm**

| | 25 | 26 | 27 | 28 | 29 | 30 |
|---|---|---|---|---|---|---|
| **7km** | 0,56 | 0,76 | 0,40 | 0,74 | 0,49 | 0,64 |
| **2.8km** | 0,56 | 0,74 | 0,45 | 0,69 | 0,51 | 0,61 |
| **1.1km** | 0,54 | 0,74 | 0,43 | 0,71 | 0,48 | 0,60 |

Figure 10: Comparison between the correlation coefficients of the three simulations for the two channels. In the tables are reported the mean values of correlation coefficient for each day.

The simulations at different resolution show almost the same pattern except for results obtained for $28^{th}/29^{th}$. For these two days the best results are obtained from COSMO-7_ITA configuration. Moreover, is visible a general good agreement with observations for periods without clouds for both channels. Instead a lower agreement between observations and synthetic satellite images characterizes cloudy periods, especially for IR 10.8 $mu$m channel.

A consistent result is also obtained in terms of RMSE (Figure 11).

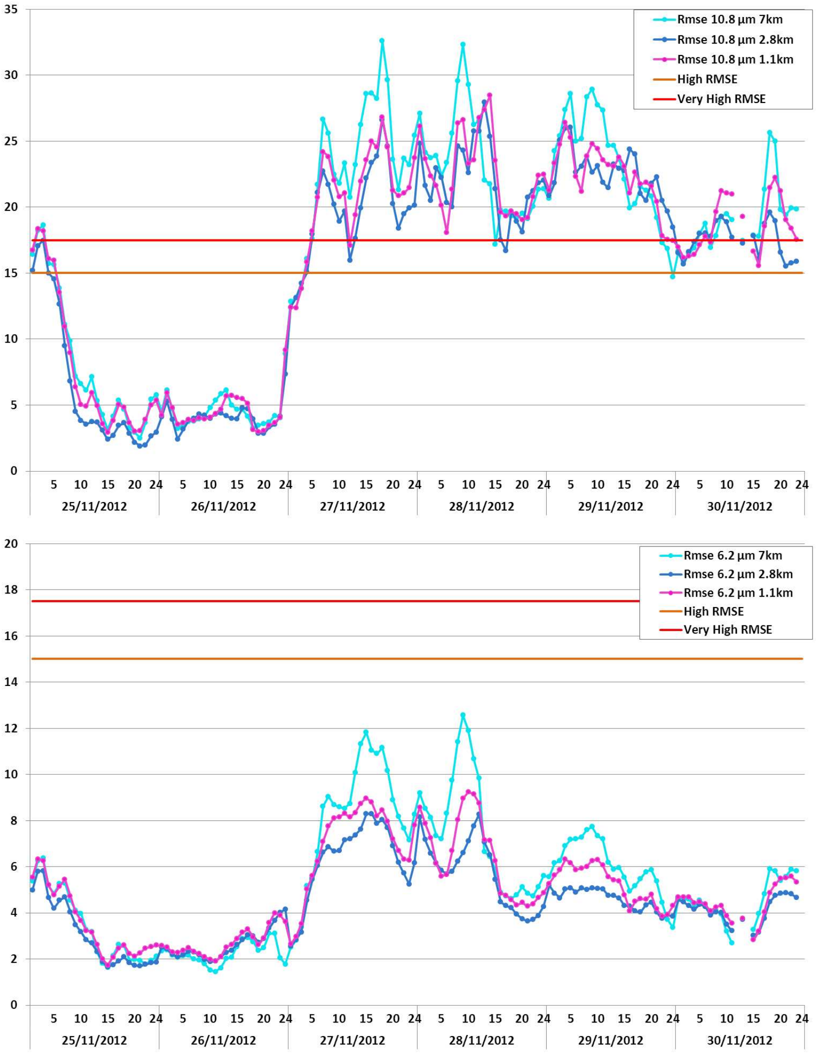


**Mean Rmse 10.8 µm**

| | 25 | 26 | 27 | 28 | 29 | 30 |
|---|---|---|---|---|---|---|
| 7km | 8,21 | 4,56 | 22,93 | 23,11 | 23,16 | 19,02 |
| 2.8km | 6,56 | 4,07 | 19,56 | 21,96 | 22,51 | 17,48 |
| 1.1km | 7,92 | 4,50 | 20,69 | 22,56 | 22,36 | 18,62 |

**Mean Rmse 6.2 µm**

| | 25 | 26 | 27 | 28 | 29 | 30 |
|---|---|---|---|---|---|---|
| 7km | 3,43 | 2,24 | 8,12 | 7,43 | 6,01 | 4,57 |
| 2.8km | 3,05 | 2,63 | 6,30 | 5,69 | 4,59 | 4,14 |
| 1.1km | 3,55 | 2,71 | 6,97 | 6,40 | 5,24 | 4,44 |

Figure 11: Comparison between the RMSE of the three simulations for the two channels. In the tables are reported the mean values of RMSE for each day.

Indeed, even in terms of RMSE the three simulations show almost the same pattern. The error is lower for periods without clouds for both channels and is higher for cloudy periods, especially for IR 10.8 $mu$m channel. Concerning the WV 6.2 $mu$m channel, instead, there is almost no error for the entire period.

An analysis in terms of statistical indices has been realized also between the two different configurations of COSMO-1_ITA, the old and the optimized one. The results are shown in Figure 12.

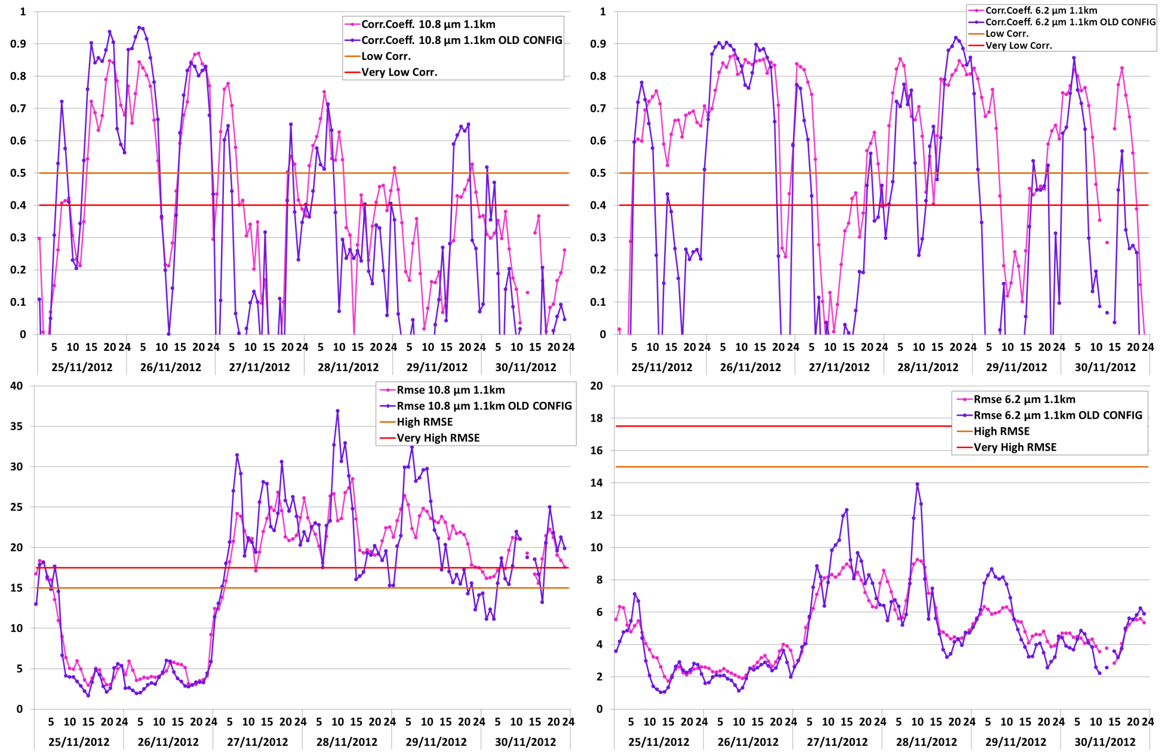


**Mean Corr.Coeff. 10.8 µm**

| | 25 | 26 | 27 | 28 | 29 | 30 |
|---|---|---|---|---|---|---|
| new | 0,46 | 0,64 | 0,36 | 0,45 | 0,29 | 0,22 |
| old | 0,50 | 0,68 | 0,15 | 0,34 | 0,17 | 0,08 |

**Mean Corr.Coeff. 6.2 µm**

| | 25 | 26 | 27 | 28 | 29 | 30 |
|---|---|---|---|---|---|---|
| new | 0,54 | 0,74 | 0,43 | 0,71 | 0,48 | 0,60 |
| old | 0,27 | 0,68 | 0,22 | 0,65 | 0,15 | 0,35 |

**Mean Rmse 10.8 µm**

| | 25 | 26 | 27 | 28 | 29 | 30 |
|---|---|---|---|---|---|---|
| new | 7,92 | 4,50 | 20,69 | 22,56 | 22,36 | 18,62 |
| old | 7,38 | 3,50 | 22,82 | 22,57 | 21,25 | 17,65 |

**Mean Rmse 6.2 µm**

| | 25 | 26 | 27 | 28 | 29 | 30 |
|---|---|---|---|---|---|---|
| new | 3,55 | 2,71 | 6,97 | 6,40 | 5,24 | 4,44 |
| old | 3,10 | 2,22 | 7,74 | 6,34 | 5,43 | 4,26 |

Figure 12: Comparison between the correlation coefficients of the three simulations for the two channels. In the tables are reported the mean values of correlation coefficient for each day.

From Figure 12 is visible a general improvement of the results with the use of the new configuration of COSMO-1_ITA. Indeed the correlation between observed and synthetic satellite images is higher and the maximum RMSE is lower than the one obtained with old configuration, for both channels.

Furthermore, soundings data have been used to analyze two particular cases: one of good agreement with observation ($26^{th}$ of November at 04UTC) and one of lower agreement ($30^{th}$ of November at 13UTC) which correspond to, respectively, high correlation (low RMSE) and low correlation (high RMSE). The evaluation of the performances for these two cases has been carried out through the use of soundings. The observed soundings are taken from the station of Pratica di Mare, that is located inside the simulation domain (Figure 13), at 00UTC and 12UTC.


Figure 13: Location of observation station of Pratica di Mare.

Simulated soundings are realized using the nearest grid point of the model to the observation station, for the different resolutions, at 00UTC and at 12UTC. The simulated soundings at 00UTC are obtained through the use of the analysis data (which in this case is the model output at 00UTC).

In Figure 14 are reported the results for the best case ($26^{th}$ of November) at 00UTC and at 12UTC. In this case COSMO-7_ITA, COSMO-2.8_ITA and COSMO-1_ITA show almost the same pattern and there's a general good agreement with the pattern of the observation soundings. For the worst case ($30^{th}$ of November, Figure 15), in the results of 00UTC the three simulated soundings show the same pattern, different from the observed one. In particular, the analysis differs for lower levels (900-700 hPa) and for middle levels (600-350 hPa). Also in the image of 12UTC the simulations show a pattern quite different from the observations, even if here the 7km simulation exhibits a different behavior compared with the others two configurations. In general, as regards the worst case, the model shows a greater error in the reproduction of the thermodynamic state of the atmosphere.

These results are in agreement with what has been already seen in Figure 10 and in Figure 11, since the best case shows good results even in terms of correlation and error, as well as the worst case shows worse results in terms of correlation and error. Therefore it is possible to say that a bad description of the state of the atmosphere through the different layers, in turn, leads to a worse quality of the forecast. Moreover, while in WV channel results are always quite good, in the IR channel error is higher, especially in cloudy periods. This could mean that the cloud is rightly localized, since the error in terms of water vapour is low, but the cloud temperature is not well identified.

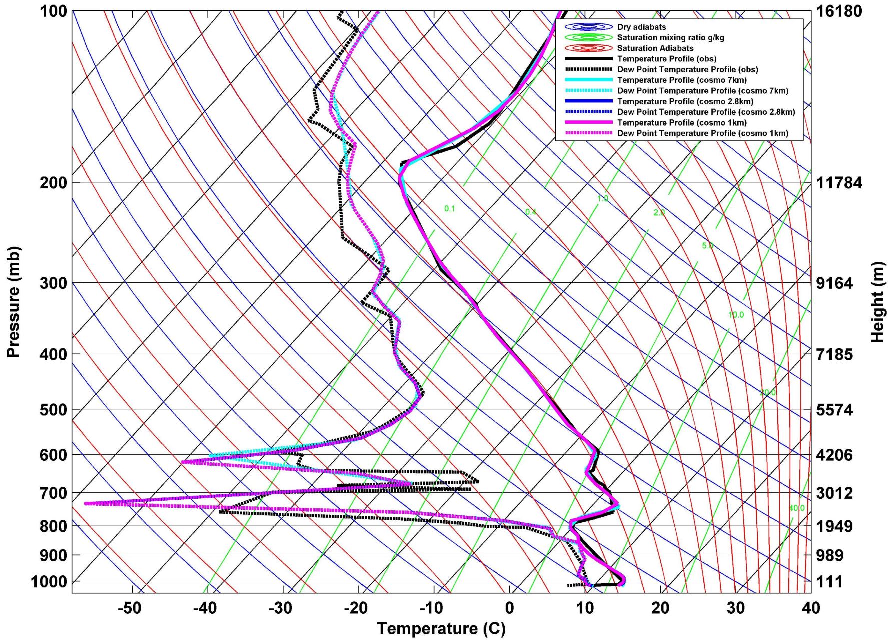


(a)

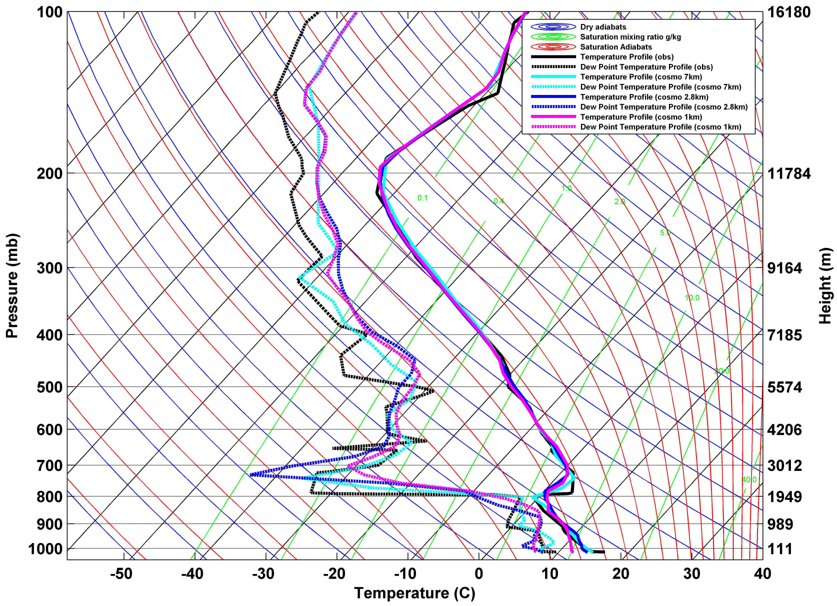


(b)

Figure 14: Comparison between observed and simulated soundings for the different simulations for 26*th* of November at 00UTC (a) and 12UTC (b).

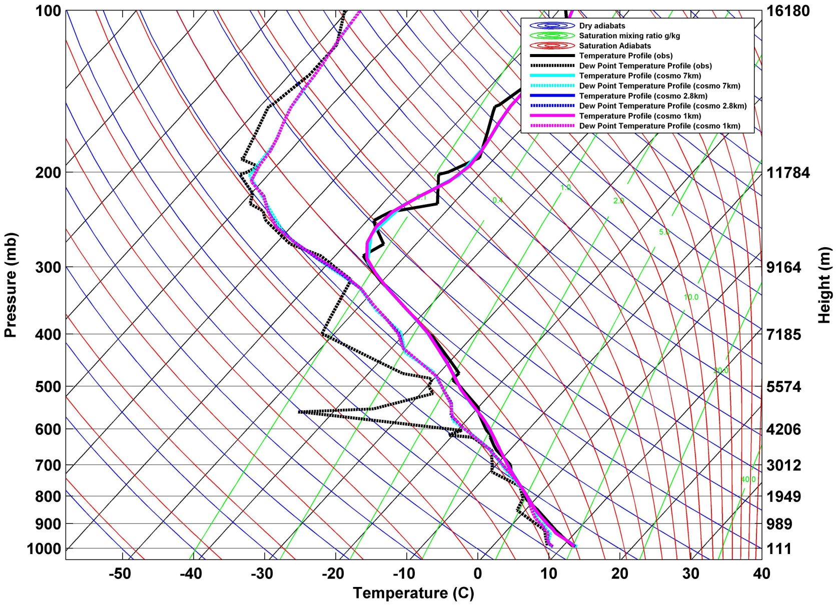


(a)

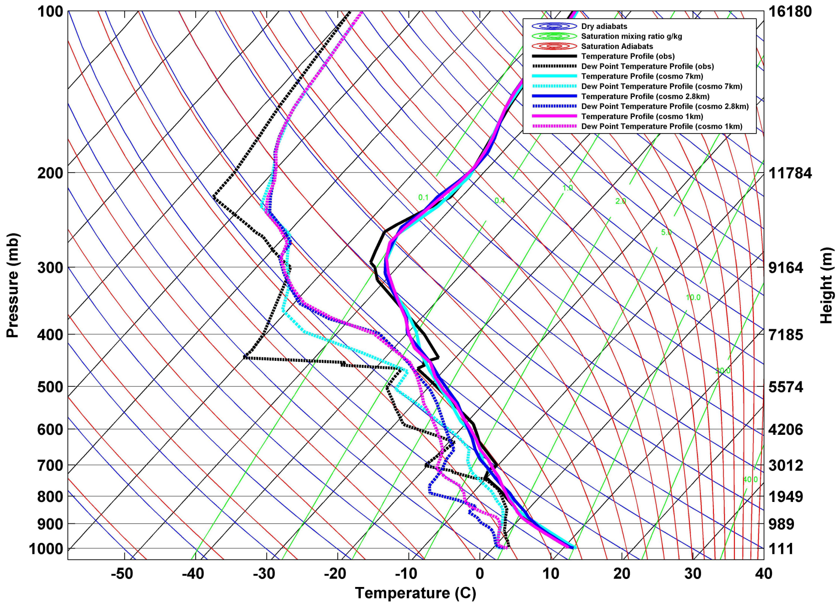


(b)

Figure 15: Comparison between observed and simulated soundings for the different simulations for 30*th* of November at 00UTC (a) and 12UTC (b).

The last analysis performed in the present work regards the study of kinetic energy spectra, used to evaluate the effective resolution of the COSMO-1_ITA simulations. A spectral decomposition was made with 2D-DCT (Denis et al., 2002) of the horizontal components of wind at different heights (200 hPa, 250 hPa, 300 hPa, 400 hPa, 500 hPa, 600 hPa, 700 hPa). The results obtained with this procedure have been avaraged daily. In Figure 16 are shown results only for 26*th* and 30*th* November, but these results are confirmed also for the other days.

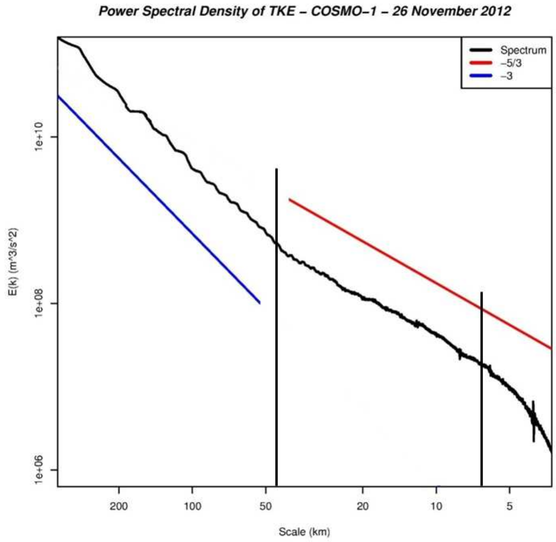


(a)

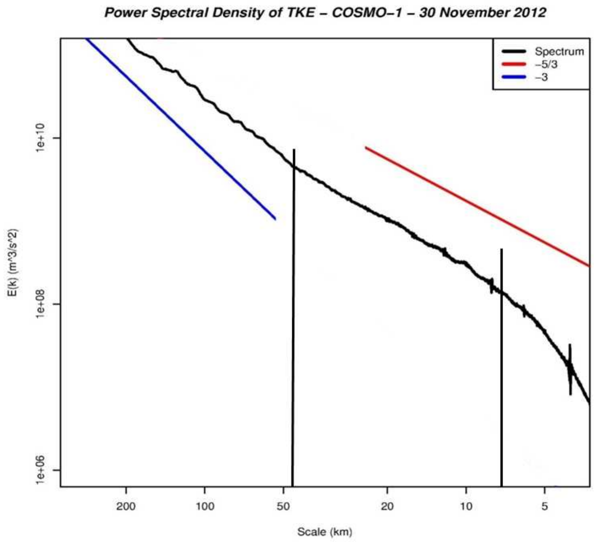


(b)

Figure 16: Power spectral density of TKE for 26 (a) and 30 (b) November.

The results are in agreement with experimental spectra by Skamarock, 2004 since for the largest spatial scale the spectral solpe is approximately -3. The transition from -3 to -5/3 is around 50 km. The loss of information is between 10 and 5 km, that is in the range of 5-10 times the nominal resolution of the model. Further experiments show that for the same test case the cofiguration at 7 km of resolution has a lower effective resolution, as expected. In Figure 17 are shown results for COSMO-7_ITA for $26th$ and $30th$ November. In this case the resolution of the model is too coarse to reproduce the -5/3 spectral slope, so it can only reproduce the -3 slope.

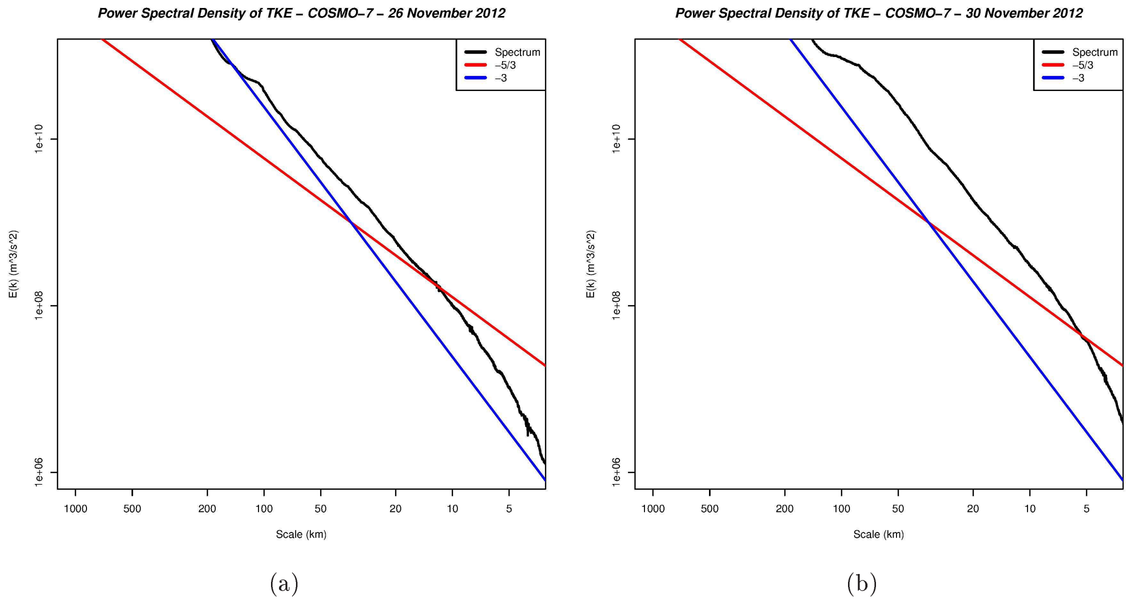


Figure 17: Power spectral density of TKE for 26 (a) and 30 (b) November for COSMO-7_ITA simulation.

## 4 Conclusion

The aim of the work was the evaluation of the performances of COSMO-1 model over the Italian domain with different kinds of observations, suitable for the high resolution of the model, and with different configurations of COSMO (different resolutions: 7 km and 2.8 km).
The behavior of COSMO-7_ITA, COSMO-2.8_ITA and COSMO-1_ITA is quite the same for almost every variable analyzed in the validation, even if, for the cloudy days analyzed, the three simulations have worst performances. In this regard it is necessary to perform further analysis, even on the longest test case, since six days are a relatively short period to make precise estimates of error. In addition, further testing should be performed also on other variables.
The analysis of kinetic energy spectra shows a good agreement with experimental spectra by Skamarock. The loss of information is between 10-5 km, which is the effective resolution of the model. Is possible to conclude that, using a higher resolution, is possible to analyze meteorological structures characterized by a higher resolution with respect to that of 7 km and 2.8 km. This confirms that the nesting strategy used is correct and an increase of resolution can increase the capacity of the model to forecast structures more localized in space and time. Anyhow this should be verified with observations suitable for the validation of such high resolutions, such as radar or non-GTS stations.

# References

[1] Reichert, B. K., Träger-Chatterjee, C. and Asmus, J., 2005: Using synthetic satellite images for automatic monitoring of NWP fields: operational applications, *Meteorol. Sat. Conf.*, EUMETSAT, Darmstadt, Germany., pp. **67-74**.

[2] Baldauf, M., 2010: Linear Stability Analysis of Runge-Kutta-Based Partial Time-Splitting Schemes for the Euler Equations, *American Meteorological Society*.

[3] M. Milelli, Sensitivity of COSMO-1 to vertical levels distribution, COSMO GM 2012, http://www.cosmo-model.org/content/consortium/generalMeetings/general2012/wg4-corso

[4] U. Schaettler, G. Doms, and C. Schraff, 2012: A Description of the Nonhydrostatic Regional, COSMO-Model Part VII: *User's Guide*.

[5] R. Saunders et al., 1999: An improved fast radiative transfer model for assimilation of satellite radiance observations, *Q. J. R. Meteorol. Soc.*

[6] R. Saunders et al., 2008: RTTOV9.1 Users Guide, EUMETSAT

[7] Skamarock, W. C., 2004: Evaluating Mesoscale NWP Models Using Kinetic Energy Spectra, *American Meteorological Society.*

[8] Errico, R. M., 1985: Spectra computed from a limited area grid, *American Meteorological Society.*

[9] Denis, B. et al., 2002: Spectral Decomposition of Two-Dimensional Atmospheric Fields on Limited-Area Domains Using the Discrete Cosine Transform (DCT), *American Meteorological Society.*